Qualitative comparisons of global ocean tide models by analysis of intersatellite ranging data

R. D. Ray,[1] S. B. Luthcke,[1] and J.-P. Boy[1,2]

Received 6 March 2009; revised 15 June 2009; accepted 2 July 2009; published 18 September 2009.

[1] Four global ocean tide models are compared in terms of their contribution to Gravity Recovery and Climate Experiment (GRACE) satellite-to-satellite tracking residuals. The residuals are computed relative to a comprehensive model of Earth's time-varying gravity, including allowance for mass motions in the atmosphere, ocean, terrestrial hydrology, and mantle, in addition to tides. For each analyzed tide model, 4 years of GRACE range rate data are processed. Range and range acceleration residuals are tidally analyzed by geographic location. All four global tide models are shown to be error prone in various ways, leaving tidally coherent residuals especially in polar regions but also in some lower-latitude regions. Considerable power in the solar semidiurnal S_2 tide in low latitudes suggests errors in our adopted model of atmospheric tides, which is based on 3 hourly European Centre for Medium-Range Weather Forecasts operational analyses. Anomalies in the μ_2 tidal constituent over some shallow seas suggest the presence of unmodeled nonlinear compound tides, in this case $2MS_2$. Similarly, anomalies in the nonlinear M_4 tide are seen if this constituent is omitted from the models. Errors in assumed seawater density may be contributing to some residuals.

Citation: Ray, R. D., S. B. Luthcke, and J.-P. Boy (2009), Qualitative comparisons of global ocean tide models by analysis of intersatellite ranging data, *J. Geophys. Res.*, *114*, C09017, doi:10.1029/2009JC005362.

1. Introduction

[2] Over the past 2 decades knowledge of global ocean tides has advanced markedly, thanks in great part to satellite altimetry. These advances have been documented by many types of tests, including comparisons of tidal models against independent tide estimates extracted from tide gauge and bottom pressure measurements [e.g., *Andersen et al.*, 1995], variance reduction tests with independent satellite altimeter data [e.g., *Dorandeu et al.*, 2000], tidal loading tests with gravimeter or other geodetic data [e.g., *Llubes and Mazzega*, 1997; *Baker and Bos*, 2003], comparisons of model tidal currents against independent point measurements at moorings and line integral measurements along long acoustic paths [*Dusahw et al.*, 1997], and comparisons of low-degree spherical harmonic coefficients with those estimated from independent satellite laser ranging data, including the geophysically important degree 2 terms [*Ray et al.*, 2001].

[3] In this paper we examine a new satellite-based test that offers a unique and complementary perspective. The two Gravity Recovery and Climate Experiment (GRACE) satellites [*Tapley et al.*, 2004], orbiting at an altitude of ~480 km, form a highly sensitive detector of mass changes in the Earth system. This is accomplished by precisely monitoring the relative distance between the two satellites [*Wolff*, 1969] by "dual-one way range" [*MacArthur and Posner*, 1985; *Dunn et al.*, 2003] using K band and Ka band frequencies. In our case the surface mass changes of interest are those caused by oceanic tides.

[4] As a test of tide models, GRACE offers some advantages over previous surface gravimeter tests [e.g., *Baker and Bos*, 2003], because it can (to within its inherent spatial resolution) more clearly delineate which regions of the ocean are causing observed anomalies in tidal gravity. It is especially valuable for its superior coverage of the data-sparse regions of the polar oceans. Moreover, its extreme sensitivity can potentially give useful new tidal information even over lower-latitude oceans that are well covered by satellite altimetry. On the other hand, the GRACE spatial resolution limits its ability to detect very short-wavelength tidal errors in models; such errors are known to be significant in shallow seas and near-coastal waters for all currently existing global models.

[5] It is already well established that GRACE is sensitive to mass fluctuations associated with ocean tides [*Ray et al.*, 2003; *Han et al.*, 2004]. Further, it is sensitive to errors in the tide models currently adopted to remove tidal effects from the GRACE ranging measurements [*Han et al.*, 2005; *Schrama et al.*, 2007; *Moore and King*, 2008]. In fact, residual tide effects can impact GRACE's ability to resolve nontidal mass motions in the Earth system, which provides an important motivation for tide model improvement.

[6] Initial efforts have begun to extract tidal signals from GRACE in order to improve the long-wavelength components of tide models, either globally or regionally [*Han et al.*, 2005, 2007]. Inversions of GRACE data to determine such corrections are extremely promising, but, like any inversion

[1]NASA Goddard Space Flight Center, Greenbelt, Maryland, USA.
[2]Also at EOST, IPGS, Strasbourg, France.

Copyright 2009 by the American Geophysical Union.
0148-0227/09/2009JC005362

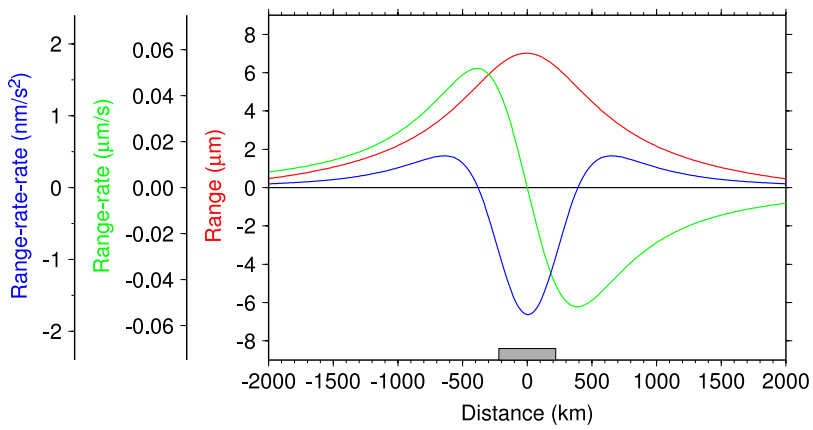

Figure 1. Theoretical range, range-rate, and range-rate-rate signals in a low-low satellite-to-satellite tracking system as it overflies (at GRACE altitude and satellite separation) a mass anomaly of 10 cm equivalent water covering an area of 2×10^5 km^2 ($4° \times 4°$ at equator). X axis denotes along-track distance from the mass anomaly.

of gravity data, issues involving ill posedness, resolution, and regularization must be addressed. We here avoid such complexities by analyzing only the basic intersatellite ranging residuals with respect to various prior models. This limits us to a qualitative analysis of tide models, as opposed to quantitative estimation in terms of sea-surface elevations. The results, however, allow straightforward intercomparison of tidal models in terms of their measurement residuals, and they shed considerable light on deficiencies in all considered models.

2. Preliminaries

[7] Figure 1 is a reminder to the reader of how the fundamental GRACE ranging signals appear in response to a fairly localized mass anomaly. This calculation is based on a simple scenario of two low-low satellites flying in a perfectly circular orbit of radius R with no nonconservative forces. In that case the range-rate $\dot{\rho}$ between the two satellites is approximately proportional to the induced potential difference at the two satellite positions (R, θ_1, φ) and (R, θ_2, φ) [*Wolff*, 1969]

$$\dot{\rho}(t) = (R/GM)^{1/2}[U(R,\theta_1,\varphi) - U(R,\theta_2,\varphi)], \qquad (1)$$

where $R(\theta_2 - \theta_1)$ is the satellite separation distance, G is the gravitational constant and M the mass of the earth. If we express the mass anomaly of Figure 1 in terms of sea-surface elevation (10 cm in this example), expanded as a spherical harmonic series

$$\zeta(\theta,\varphi) = \sum_{n,m} z_{nm} Y_n^m(\theta,\varphi), \qquad (2)$$

the potential U is then given by [e.g., *Lambeck*, 1988]

$$U(r,\theta,\varphi) = 4\pi G a \rho_w \sum_{n,m} \frac{1+k'_n}{2n+1}\left(\frac{a}{r}\right)^{n+1} z_{nm} Y_n^m(\theta,\varphi), \qquad (3)$$

where ρ_w is the mean density of seawater, a is the radius of the earth, and k'_n are loading Love numbers. If ζ represents a tidal oscillation, then z_{nm} is a function of time with tidal periodicity.

[8] As Figure 1 shows, perturbations in range and range acceleration tend toward maximum amplitude directly over a causative body, although with possible side lobes. Range-rate signals are always offset with a zero crossing over the causative body. For this reason most (but not all) of our analyses of GRACE residuals are done in terms of range and range acceleration. As seen below, both types of signals require filtering to isolate local anomalies, so the information in each tends to be complementary and not necessarily redundant.

3. GRACE Data Processing

[9] We begin with Level 1B GRACE data produced at the Jet Propulsion Laboratory [*Case et al.*, 2004]. These data sets include filtered accelerometer, range, and range-rate measurements every 5 s along satellite arcs. We calibrate the accelerometry as described by *Luthcke et al.* [2006], adjusting bias, scale, and orbital resonance parameters in a least squares fit to both the range-rate data and a "reduced dynamic" orbit solution, with weighting appropriate to noise levels in each data type.

3.1. Adopted Models

[10] We have endeavored to make the satellite force models needed for these calculations as complete as possible, one benefit being that small differences in tide models should then be more easily isolated. Static gravity is modeled with the GGM02C model [*Tapley et al.*, 2005]. Time-variable gravity is modeled from multiple sources, as follows.

3.1.1. Atmosphere

[11] Variable atmospheric mass is modeled with 3 hourly operational analysis outputs from the European Centre for Medium-Range Weather Forecasting (ECMWF) [*Klinker et al.*, 2000]. The 3 hourly data are linearly interpolated to the epoch of interest. These data, in contrast to the classical 6 hourly sampling, allows for adequate sampling of the diurnal,

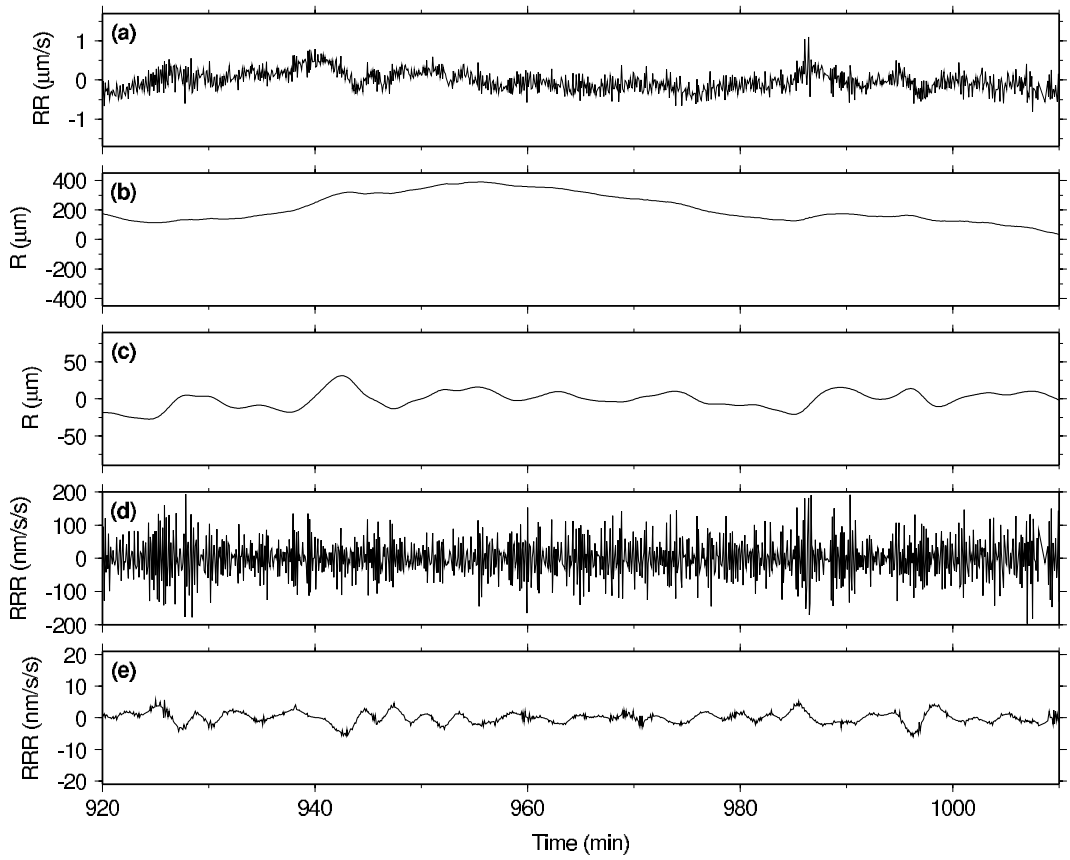

Figure 2. GRACE residuals for a 90-min arc (approximately 1 orbital revolution) beginning 4 April 2005 at 1520 UT. Data rate is one measurement every 5 s. Quantities are (a) range rate (μm s^{-1}); (b) range (μm), from time integration of range rates; (c) high-pass-filtered ranges; (d) range rate rate (nm s^{-2}), from simple finite differencing of original range rates; and (e) low-pass-filtered range rate rates.

semidiurnal, and terdiurnal atmospheric tides. Note that the ECMWF spatial resolution increased in February 2006, from about 80 (T255) to 25 km (T799), so the later data may show some level of improved realism.

3.1.2. Oceans (Nontidal)

[12] Variable oceanic mass is modeled with 6-hour outputs from the Toulouse Unstructured Grid Ocean model (T-UGO), which is run in barotropic mode and is forced by 6 hourly ECMWF surface pressures and winds [*Carrère and Lyard*, 2003]. Mean S_1 and S_2 tides, adjusted by least squares fitting over the 1997–2007 period, have been removed to avoid double counting with the radiational components of the ocean tide models.

3.1.3. Land Hydrology

[13] Variable terrestrial water storage on land is modeled with outputs from the Global Land Data Assimilation System (GLDAS), using the Noah land-surface model [*Rodell et al.*, 2004]. These data are available every 3 hours on a global 0.25° grid. We mask out regions of ice sheets and major mountain glaciers because of a lack of dynamic ice modeling in GLDAS.

3.1.4. Mantle Rebound

[14] Secular changes in mass owing to glacial isostatic adjustment are modeled by using ICE-5G (VM2) of *Peltier* [2004]. Our models for mass variations due to tides are described in detail in section 4.

[15] All these sources of time-varying gravity are expanded in spherical harmonics and used as adjustments to static GGM02C Stokes geopotential coefficients. These are then used to compute satellite-to-satellite range rates, parameterized as time-varying baseline changes between the two satellites [*Rowlands et al.*, 2002]. The modeled range rates form the basis for computing our measurement residuals.

3.2. Filtering

[16] Figure 2a shows real GRACE residuals along an arc of roughly one complete orbital revolution. Although some level of noise is apparent, signals with amplitudes well below 0.5 μm s^{-1} can easily be discerned in the time series. Figures 2b and 2d show corresponding range and range-rate-rate residuals, formed by simple trapezoidal integration and finite differences, respectively. As is well known, integration inflates low-frequency errors and differentiation inflates high-frequency errors, which is plainly evident in the two curves. We therefore high-pass filter the former and low-pass filter the latter. The filtered time series (Figures 2c and 2e) form the basis for the remainder of our analysis.

[17] Our nominal low-cut filter has a cutoff frequency of 5×10^{-4} Hz; the high-cut filter cutoff is 6×10^{-3} Hz and is combined with an 11-point median filter. The effect on the spectrum of the range-rate time series is shown in Figure 3. No claim of optimality can be made for these filters. They

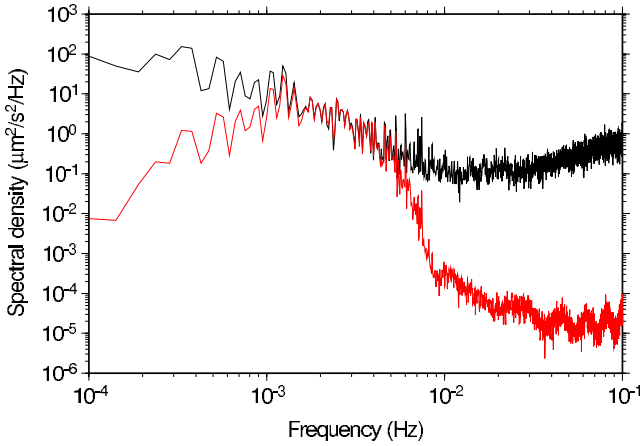

Figure 3. Spectrum (in black) of the range-rate residuals for 4 April 2005, a segment of which is shown in Figure 2a. Red shows the spectrum after low-pass and high-pass filtering (combined into one diagram for illustration purposes). The filtering is necessary to compute range and range-acceleration time series. Frequency of 10^{-3} Hz corresponds to a wavelength of approximately 7000 km. A 1-cycle/revolution signal would appear at frequency 1.77×10^{-4} Hz.

were designed subjectively. However, the original range-rate spectrum appears abnormally blue at high frequencies, so the high-frequency cutoff seems reasonable. Placement of the low-frequency cutoff is less easily determined; it may be removing true signal, although most of that signal is unlikely to be tidal since it is of hemispheric wavelengths and longer.

[18] One undesirable consequence of filtering range residuals is that, given the nature of high-pass filters, any given range anomaly is likely to develop small side lobes, similar to that already expected for range acceleration (Figure 1). Evidence of this is noted below.

4. Tide Models

[19] In this work we compare four different global tide models by running through the complete data-processing scheme outlined in section 3 and analyzing the resulting signals in the ranging residuals. The selected models are by no means a comprehensive compilation of all available models, but they do include those that have been most commonly employed by groups processing GRACE data. The models examined are GOT00.2, GOT4.7 (both successive updates to *Ray* [1999]), FES2004 [*Lyard et al.*, 2006], and TPXO7.1 (an update to that presented by *Egbert and Erofeeva* [2002]). The most recent releases of GRACE Level 2 data (e.g., release 4) by the project teams have employed the FES2004 model, *Luthcke et al.* [2006] used GOT00, and *Luthcke et al.* [2008] used GOT4.7.

[20] The released tide models are given in terms of gridded global arrays of amplitude and phase for eight (sometimes more) major tidal constituents. We here account for 16 additional minor tides by inference from the given major tidal admittances, a procedure which is generally acceptable for deep ocean tides [*Munk and Cartwright*, 1966] if allowance is made for radiational effects in a few constituents [*Cartwright and Ray*, 1994; *Arbic*, 2005]. These inference methods are invalid in some shallow seas or under floating ice shelves [e.g., *Pedley et al.*, 1986] where nonlinear interactions can appear, but these tend to be shorter-wavelength waves less observable at GRACE altitudes (but see discussion below). Lunar constituents are, of course, adjusted for nodal and perigee modulations where appropriate. Our method for accounting for minor tidal lines is in essence equivalent to the convolution methodology of *Desai and Yuan* [2006], although the mathematical forms of our admittance interpolations are slightly different (e.g., piecewise linear versus sinusoidal) and the implementations are considerably different; largest differences will occur when admittances are extrapolated to the edges of tidal bands, for constituents like $2Q_1$ and OO_1, but these constituents are very small.

Table 1. GRACE Range-Rate RMS Residuals[a]

	2003	2004	2005	2006	2007	5 Year Total
GOT00.2	0.2361	0.2495	0.2315	0.2693	0.2696	0.2498
TPXO7.1	0.2359	0.2498	0.2308	**0.2670**	0.2694	0.2490
FES2004	**0.2341**	**0.2480**	**0.2307**	0.2671	0.2680	**0.2482**
GOT4.7	**0.2341**	0.2485	0.2308	0.2671	**0.2677**	0.2483

[a]Values are given in μm s^{-1}. Values given in bold mark the smallest RMS in each year.

[21] Most released tide models include the long-period constituents Mf and Mm (FES2004 includes the termonthly Mt and quarter monthly MSq as well). The remainder of the long-period tidal band is here assumed to maintain an equilibrium response with its forcing, consistent with mass conservation, loading, and self-attraction [e.g., *Agnew and Farrell*, 1978].

[22] To compute the gravitational effects of tides we expand all major and minor constituents in terms of spherical harmonics of the form (2–3). Major tides are expanded to degree 70, which prelaunch calculations suggested was sufficient [e.g., *Ray et al.*, 2003]. (Note, however, that M. Watkins (personal communication, 2007) has seen evidence of small tidal effects in GRACE through degree 90.) We expand minor diurnal and semidiurnal tides to degree 50 and long-period tides to degree 20 or 30, depending on amplitude.

[23] Atmospheric tides are incorporated automatically by our use of the ECMWF model for general atmospheric mass variability, as noted in section 3. In the past [e.g., *Luthcke et al.*, 2006] we have used a (monthly) mean climatology of atmospheric tides derived from 6 hourly ECMWF data [*Ray and Ponte*, 2003]. In principle the use of direct 3 hourly ECMWF is preferable for the following reasons: (1) there is no longer need to make assumptions about semidiurnal phase propagation to overcome the inadequate 6-hour temporal sampling [*Van den Dool et al.*, 1997]; (2) temporal variability not captured in climatological means can be accounted for; and (3) lunar atmospheric tides are also incorporated, not because ECMWF models the gravitational tidal forcing of the atmosphere but rather because the lunar tides leak in via

Table 2. Alias Periods for Semidiurnal Tides as Sampled by GRACE

Constituent	Frequency (°/h)	Alias (days)
M_2	28.984104	13.5
T_2	29.958933	111.8
S_2	30.000000	161.0
R_2	30.041066	288.0
K_2	30.082137	1362.7

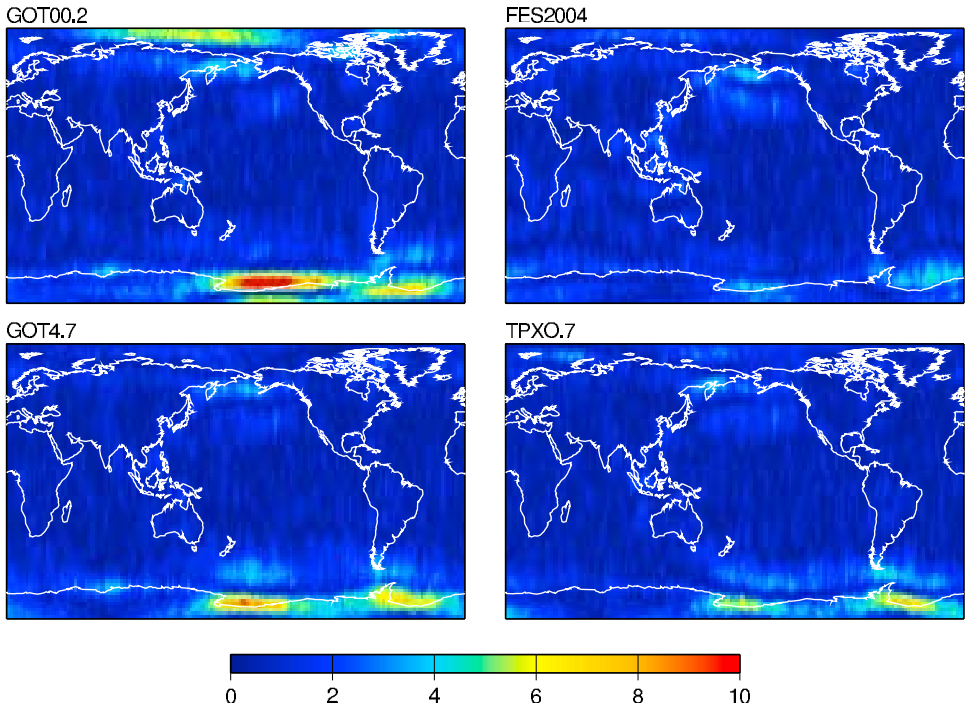

Figure 4. Amplitudes (μm) at the O_1 tidal frequency in 4 years of GRACE range residuals, based on four different prior models of ocean tides. Locations having significant amplitudes suggest errors in tide models.

assimilation of surface barometer observations [*Hsu and Hoskins*, 1989]. Below we show evidence that this air-tide modeling is not perfect.

[24] For completeness we note that the Earth's body tides are modeled according to *McCarthy and Petit* [2003, section 6.1], with frequency-dependent anelastic Love numbers for the degree 2 components of the tidal potential and a frequency-independent elastic Love number for the degree 3 components.

5. Results

[25] These results are based on 4 years of GRACE satellite-to-satellite ranging data, from April 2003 to April 2007. The

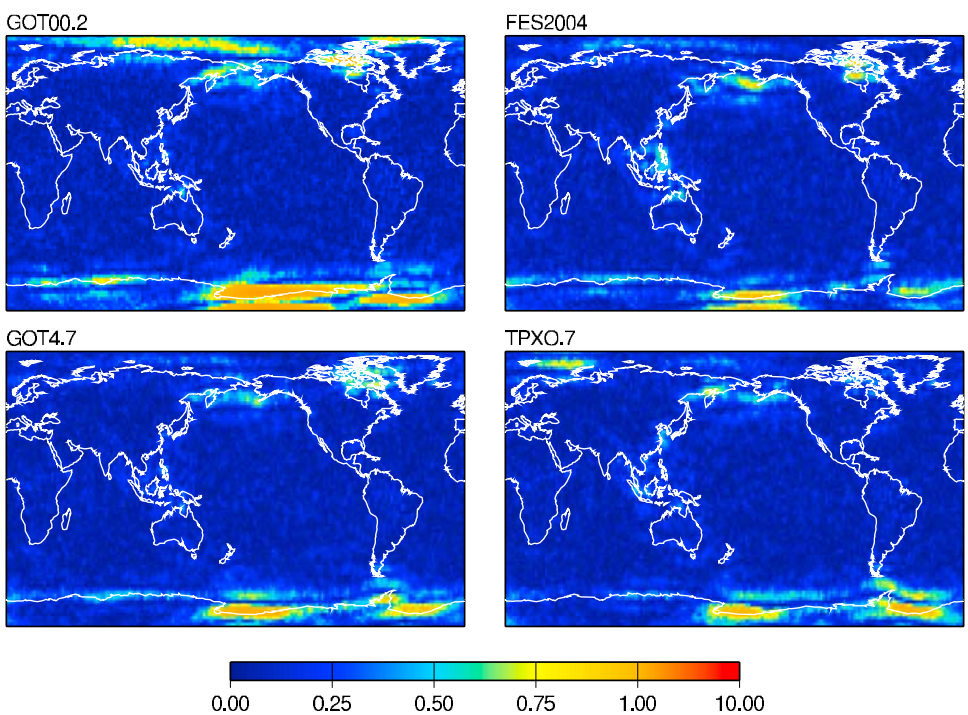

Figure 5. Amplitudes (nm s^{-2}) at the O_1 tidal frequency in 4 years of GRACE range-rate-rate residuals, based on four different prior models of ocean tides.

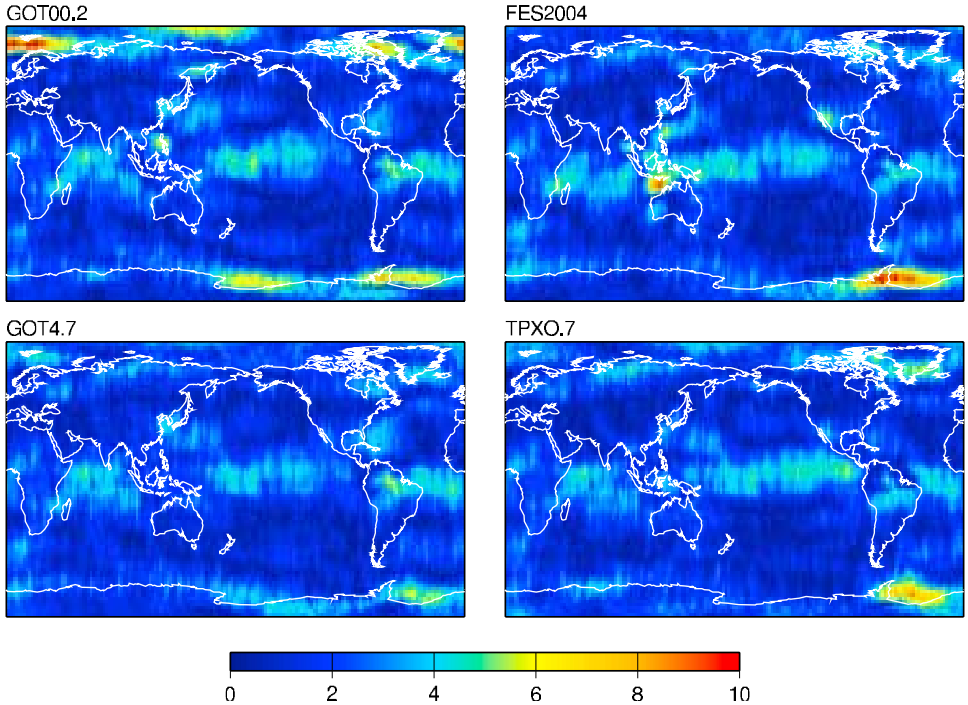

Figure 6. As in Figure 4 except for the S_2 constituent. The large low-latitude bands are suggestive of errors in the ECMWF atmospheric S_2 tide which was used for all four cases.

data have been processed four times through our entire processing scheme, beginning with accelerometry calibration, keeping all geophysical modeling fixed except the ocean tide model.

5.1. Statistics of Residuals

[26] As a simple global summary Table 1 tabulates the final root-mean-square (RMS) statistics of range-rate residuals for each adopted tide model, divided out by year. It is rather surprising how close are the results, with models sometimes in agreement to four significant figures. As a test for selecting which model may be preferable, Table 1 is thus not so useful, although it does suggest that GOT00.2 can now (rightly) be considered obsolete.

5.2. Tidal Analysis of Residuals

[27] A far more enlightening analysis of the residuals is obtained by treating them as almost a form of satellite altimetry to be geographically binned and tidally analyzed. This exploits the fact that anomalies in range and range acceleration tend to be localized over causative bodies. This section discusses the results of such analyses when binning data into small overlapping regions of size 5° (longitude) by 2° (latitude) and harmonically analyzing the data at a number of tidal frequencies.

[28] Like any satellite in its altitude range, GRACE aliases tidal signals into longer periods, which range anywhere from days to years [*Ray and Luthcke*, 2006]. Any successful tidal analysis depends on noise remaining incoherent at tidal periods. When aliasing occurs this becomes less likely, because some alias periods can be long compared with the time series length or they may fall near periods of large nontidal variability (e.g., seasonal). For GRACE a number of aliased tidal constituents fall into one or the other of these categories. They are generally solar constituents, including the partly solar K_1 and K_2.

[29] Thus, to interpret the following results it is helpful to recall some aspects of tidal aliasing in GRACE [*Ray and Luthcke*, 2006, section 2]. Nontidal variability occurring at tidal alias frequencies will tend to corrupt analyses of semidiurnal constituents more than diurnal constituents. For the former, on account of the Earth's two-sided tidal bulge,

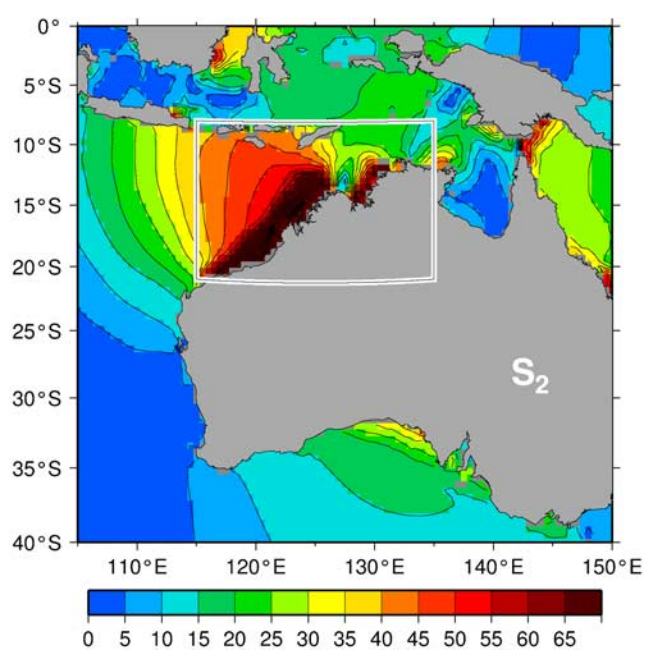

Figure 7. Amplitudes (cm) of the S_2 ocean tide off Australia. The box shows the region highlighted in Figure 8.

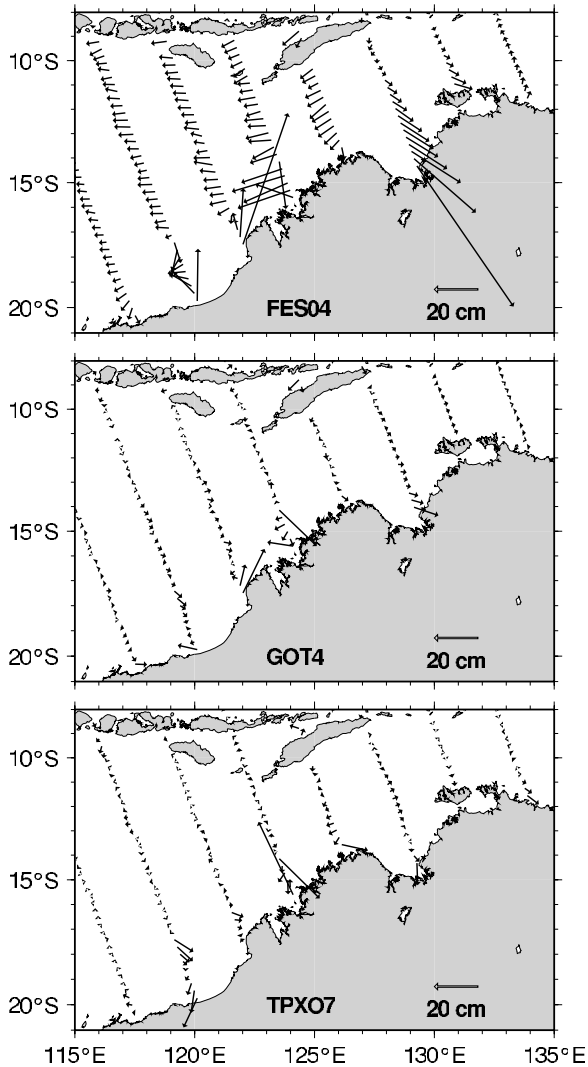

Figure 8. Vector differences between S_2 tides estimated along eight Topex/Poseidon tracks and models FES2004, GOT4.7, and TPXO.7. Note scale bar at lower right. The large residuals in FES2004 are consistent with those in Figure 6.

ascending and descending GRACE arcs are nearly in phase, with nearly identical sampling of any aliased energy. In contrast, for diurnal tides ascending and descending arcs are nearly out of phase [see *Ray and Luthcke*, 2006, Figure 1] thus tending to break correlations with (unaliased) nontidal energy. Table 2 lists the alias periods of the most significant semidiurnal tides [see *Ray and Luthcke*, 2006]. At 3.7 years, K_2, we find, is so dominated by nontidal energy that any true tidal signals in our results are difficult to recognize. We find, as expected, diurnal constituents to be less affected, with one exception. The diurnal K_1 is a special case, because its alias period is so long (7.5 years) that our 4-year analysis results for it are nonsensical. We therefore begin discussion with the second largest diurnal tide.

[30] Figures 4 and 5 show results for the principal lunar diurnal tide O_1 in (high-pass filtered) residuals of intersatellite range and (low-pass filtered) residuals of range acceleration, respectively. Locations in these maps having significant amplitude (relative to background noise) are without exception locations of known tidal modeling problems, especially in polar seas where satellite altimetry is lacking. The GOT00 model displays large errors in the Arctic Ocean north of Siberia, but these errors are evidently much reduced in the other three models. Both the Bering Sea and Okhotsk Sea are regions having relatively large O_1 tidal amplitudes yet are somewhat poorly sampled by altimetry owing to persistent ice contamination; errors in both seas are therefore not unexpected. All four models display errors near Antarctica, especially in the Ross and Weddell Seas. FES2004 looks superior in this region, although FES2004 anomalies are more noticeable in range rate rate (Figure 5) than in range (Figure 4). Also apparent in Figures 4 and 5 is a suggestion of side lobes in the vicinities of large anomalies. This appears most pronounced in GOT4.7 and TPXO.7 north of the Ross and Weddell Seas.

[31] Figure 6 shows similar results for the principal semidiurnal solar constituent S_2. The results appear much noisier, with significant power evident in lower latitudes, especially in a pronounced band along the equator. The source of this band is almost surely errors in the S_2 atmospheric tide, which peaks along the equator. The same air-tide model is used in all four panels of Figure 6, and indeed the band appears similar, but not identical, in all (TPXO.7 appears most different). The band is not due to errors from mismodeling the ocean's response to the air tide, because that response is highly dynamic, not confined to the tropics, and, in fact, quite similar to the ocean's response to the S_2 tidal potential [*Arbic*, 2005]. The band could arise if modelers assimilate satellite altimeter data while mistakenly applying an "inverted barometer" correction with S_2 air tides included, but that has not been done in either GOT or TPXO models (we cannot comment on FES). An unusual aspect of this band is its nearly complete disappearance over Africa, but not South America; however, part of the signal over South America may well arise from true 160-day variability in hydrology that is unaccounted for by GLDAS (160 days is the S_2 alias in GRACE, see Table 2) and not necessarily from S_2. In any event, this band of S_2 power in the residuals could contribute to the 160-day oscillations seen in GRACE solutions for the zonal J_2 gravity coefficient (e.g., *Chen and Wilson* [2008], who attribute the J_2 oscillations to ocean-tide errors).

[32] Figure 6 also shows a significant S_2 error off northwest Australia in FES2004, but not in the other models. This has been previously reported by others [e.g., *Schrama et al.*, 2007; *Moore and King*, 2008]. That region off Australia experiences very large semidiurnal tides (Figure 7), with S_2 amplitudes exceeding one meter along a long section of coastline. As a complementary and independent analysis Figure 8 shows vector differences in this region between S_2 tides estimated point by point along Topex/Poseidon tracks [e.g., *Carrère et al.*, 2004] and three of our four tidal models. Large vector discrepancies are again seen in FES2004, especially in the southeastern Timor Sea just west of Darwin where differences with Topex/Poseidon data reach one meter. With two independent space-geodetic systems showing consistent discrepancies, it seems clear that FES2004 is in error in this region but only for the S_2 constituent (and possibly K_2).

[33] Figure 9 shows the principal lunar constituent M_2. As before, anomalies in polar regions are large, although FES2004 is clearly superior around Antarctica and TPXO7 appears best in the Ross Sea area. TPXO7 also appears best in

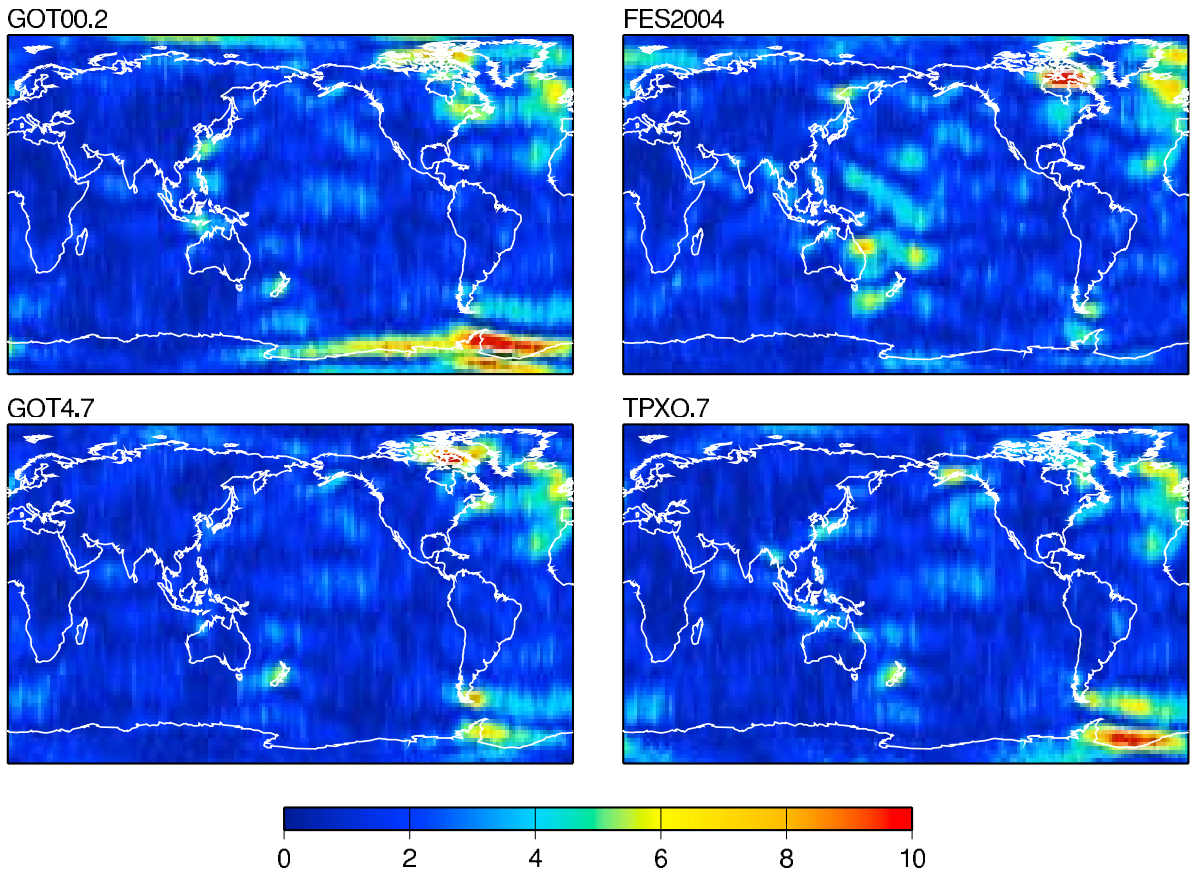

Figure 9. As in Figure 4 except for the M_2 constituent.

Hudson Bay, although it still has noticeable anomalies in Hudson Strait, an area of inordinately large tides. In addition to the relatively large anomalies in polar regions, there are a number of interesting lower-latitude anomalies. All show problems near New Zealand, a region of rapid M_2 phase changes, and southern Patagonia, a region of large, short-wavelength tides. FES2004 shows a relatively large anomaly near the Australian Great Barrier Reef; TPXO7 somewhat less so. GOT4.7 is anomalous off Maine and Nova Scotia; FES2004 not at all. Figure 9 clearly highlights our conclusion, no global tide model is without problems for processing GRACE data.

[34] One of the most surprising features of Figure 9 is that all four models show relatively large anomalies in the eastern North Atlantic Ocean. While this is a region of fairly large M_2 amplitudes, it is also well covered by high-quality satellite altimetry. One naturally wonders if some systematic error, either in GRACE or in the altimetry, could account for this. One possibility stems from equation (3), where the ocean's density has been taken as constant. More accurate would be to allow the spherical harmonic coefficients z_{nm} to represent elevation $\times$ density. The error committed by assuming constant seawater density can be evaluated by computing

$$H(\theta, \varphi)[\bar{\rho}(\theta, \varphi) - 1031], \tag{4}$$

where H is the amplitude of M_2, $\bar{\rho}$ is the mean density of the ocean water column at any location, and 1031 is the constant mean seawater density assumed by our orbit determination codes. Figure 10 shows the quantity (4) geographically, where we have evaluated $\bar{\rho}$ from the World Ocean Atlas. The largest density errors do include a region around Britain and extending west of Spain, so it is possible that these do contribute to the observed M_2 residuals, but they cannot explain the residuals over the much larger region of the eastern North Atlantic depicted in Figure 9.

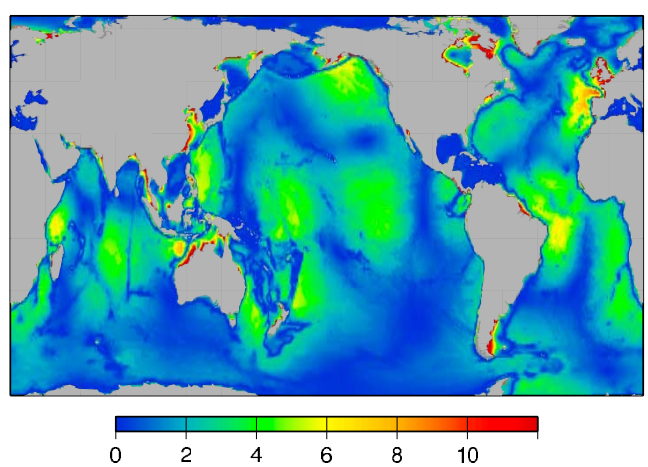

Figure 10. Magnitude of errors, according to expression (4), committed by assuming a global constant seawater density of 1031 kg m^{-3}. Units are those of surface density (kg m^{-2}).

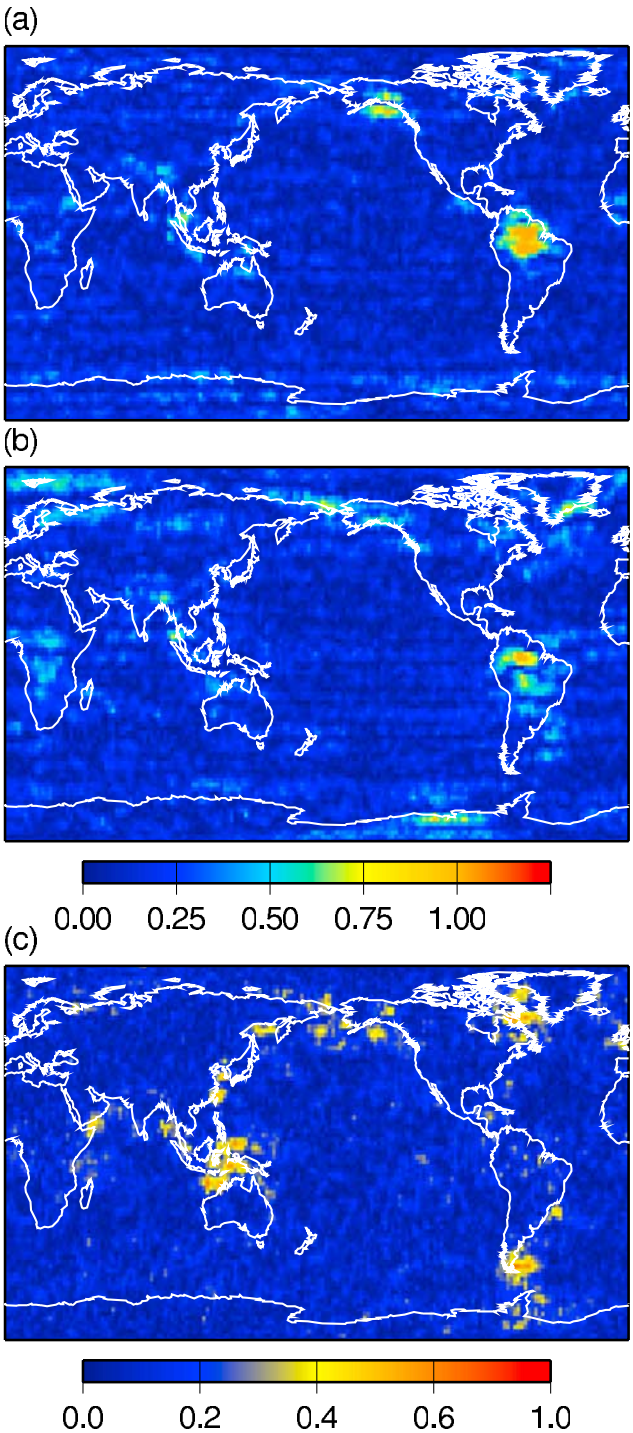

Figure 11. Amplitudes (nm s^{-2}) of range-rate-rate GRACE residuals at the tidal frequencies (a) S_1, (b) R_2, and (c) μ_2. The latter frequency coincides with that of the compound tide $2MS_2$.

[35] A preliminary inversion of the GRACE M_2 tidal residuals to determine adjustments to sea surface elevations, which at this point is still too uncertain to publish, does nonetheless suggest one possible explanation. The M_2 errors may be a series of fairly localized errors that merge together owing to GRACE's limited spatial resolving power. Our inversion places large errors off southeastern Greenland, which is perennially ice covered, off southern Ireland, and off the Faeroe Islands. Further investigation is clearly warranted.

[36] In addition to the constituents already described we have solved for a number of others. Space precludes a detailed discussion, but in Figure 11 we show some of the more interesting ones for the GOT4.7 model. Figure 11a for constituent S_1 clearly shows errors in both ocean and air tides. The latter must account for the anomalies over South America, similar to those found for S_2. The anomaly in the Gulf of Alaska, however, is undoubtedly oceanic in origin, since this is a region of some of the largest S_1 ocean tides [*Ray and Egbert*, 2004, Figure 3].

[37] The interpretation of Figure 11b, showing constituent R_2, is less clear-cut. The frequencies of R_2 and T_2 are 1 cpy away from S_2, so both constituents pick up seasonal variations in the latter, which are significant in atmospheric tides. This is possibly the source of anomalies over South America and Africa. However, these anomalies are more likely due to mismodeled hydrological changes at the R_2 alias of 288 days (Table 2). Examination of T_2 (not shown) shows features similar to Figure 11b but with less power, which might be expected if aliasing is the source, because the T_2 alias period of 112 days is much shorter than the R_2 alias. On the other hand, the R_2 air tide induces a significant radiational component in the R_2 ocean tide, which could be the source of some of the ocean anomalies. Our admittance methods for inferring R_2 (and T_2) from S_2 ignore this radiational component.

[38] Finally, Figure 11c shows the constituent μ_2, with anomalies evident in a number of shallow seas, especially near Indonesia. This suggests that the errors may actually be induced by the nonlinear compound tide $2MS_2$, whose frequency coincides with μ_2. Supporting this interpretation is the fact that a similar diagram for $2N_2$ shows almost no anomalies, yet $2N_2$ is only marginally weaker than the linear μ_2. We find no significant anomalies for the nonlinear overtide M_4 in GOT4.7, but unlike $2MS_2$, M_4 is included in the released GOT4.7 model. It is not included in GOT00, however, and M_4 range acceleration residuals for GOT00 (not shown) are very evident on the Patagonian Shelf, a region of very strong (reaching 30 cm) M_4 amplitudes. We find no evidence of any significant anomalies in the third degree M_3 constituent, even though it has isolated shelf resonances of 5–10 cm amplitude [e.g., *Huthnance*, 1980] which are not included in any of our tested models.

6. Implications

[39] None of the four global ocean tide models examined in this paper can be considered perfect for use in processing GRACE data, since each generates tidally coherent residuals in GRACE's fundamental satellite-to-satellite measurements. Each tide model has flaws in certain regions or certain constituents, and all of them require improvement in polar regions.

[40] Moreover, the atmospheric tide model used here is also found to be far from perfect. More work is needed to analyze the tides in the 3-hour ECMWF product that we adopted here and to compare these with the tidal fields used by other GRACE processing teams. Even more useful for gauging accuracy would be comparisons with surface

barometer data [e.g., *Ray*, 2001]. Unfortunately, there are hardly any good barometer stations over the region of South America where Figure 11a suggests possible air-tide errors [*Ray*, 2001]. Mismodeling temporal variability in air tides could possibly account for our results for R_2 (which acts to modulate S_2 at the annual cycle). Variability at shorter and longer periods is also known to occur, and more work is needed to understand the errors induced by such effects.

[41] If the residuals seen in the μ_2 constituent (Figure 11) are indeed due to the presence of the unmodeled compound $2MS_2$ tide, then it implies a need to reexamine the methods used in shallow seas for inferring minor tides from major tide admittances in the presence of nonlinearity. The latest global models already include the overtide M_4, and these results suggest extending such work to other nonlinear constituents. Local tide models that include compound tides already exist in many regions of the world, of course, and these could be readily adopted in GRACE modeling after appropriate testing.

[42] While we have tested four commonly employed global models, new models continue to appear, for example, the recently released EOT08a model [*Savcenko and Bosch*, 2008], which we have not yet examined. Savcenko and Bosch start with the FES2004 model and compute adjustments to it on the basis of data from multiple satellite altimeters. Presumably their adjustments rectify problems such as those seen in Figure 8, but owing to a lack of data they cannot correct the large errors in polar regions.

[43] At this stage it seems appropriate to exploit some of the local modeling efforts that have been undertaken in polar regions [e.g., *Padman et al.*, 2008], on the basis of a comprehensive approach of correcting bathymetry and ice-grounding geometry to improve realism of the hydrodynamic modeling and incorporating a variety of old and new data for constraints, such as ICESat laser altimetry. Note that Padman et al. use TPXO7 at open boundaries, so the local and global models could be immediately merged to produce a consistent, revised, global data set. In addition, of course, GRACE itself provides new long-wavelength constraints on polar tides [*Han et al.*, 2007], which can be incorporated into global models by appropriate assimilation methods.

[44] **Acknowledgments.** We thank D. Rowlands and S. Bettadpur for useful discussions. This work was supported by the National Aeronautics and Space Administration's GRACE project.

References

Agnew, D. C., and W. E. Farrell (1978), Self-consistent equilibrium ocean tides, *Geophys. J. R. Astro. Soc.*, *55*, 171–181.

Andersen, O. B., P. L. Woodworth, and R. A. Flather (1995), Intercomparison of recent ocean tide models, *J. Geophys. Res.*, *100*, 25,261–25,282.

Arbic, B. K. (2005), Atmospheric forcing of the oceanic semidiurnal tide, *Geophys. Res. Lett.*, *32*, L02610, doi:10.1029/2004GL021668.

Baker, T. F., and M. S. Bos (2003), Validating Earth and ocean tide models using tidal gravity measurements, *Geophys. J. Int.*, *152*, 468–485.

Carrère, L., and F. Lyard (2003), Modeling the barotropic response of the global ocean to atmospheric wind and pressure forcing, *Geophys. Res. Lett.*, *30*(6), 1275, doi:10.1029/2002GL016473.

Carrère, L., C. Le Provost, and F. Lyard (2004), On the statistical stability of the M2 barotropic and baroclinic tidal characteristics from along-track Topex/Poseidon satellite altimetry analysis, *J. Geophys. Res.*, *109*, C03033, doi:10.1029/2003JC001873.

Cartwright, D. E., and R. D. Ray (1994), On the radiational anomaly in the global ocean tide, with reference to satellite altimetry, *Oceanol. Acta*, *17*, 453–459.

Case, K., G. L. H. Kruizinga, and S. C. Wu (2004), GRACE level 1B data product user handbook, *Rep. JPL D-22027*, Jet Propul. Lab., Pasadena, Calif.

Chen, J. L., and C. R. Wilson (2008), Low degree gravity changes from GRACE, Earth rotation, geophysical models, and satellite laser ranging, *J. Geophys. Res.*, *113*, B06402, doi:10.1029/2007JB005397.

Desai, S. D., and D. N. Yuan (2006), Application of the convolution formalism to the ocean tide potential: Results from GRACE, *J. Geophys. Res.*, *111*, C06023, doi:10.1029/2005JC003361.

Dorandeu, J., M. Ablain, and F. Lefèvre (2000), New tide models evaluation, *AVISO Rep. AVI-NT-011-5243*, 44 pp., Coll. Localisation Satell., Ramonville Saint-Agne, France.

Dunn, C., et al. (2003), Instrument of GRACE: GPS augments gravity measurements, *GPS World*, *14*, 16–28.

Dusahw, B. D., G. D. Egbert, P. F. Worcester, B. D. Cornuelle, B. M. Howe, and K. Metzger (1997), A Topex/Poseidon global tide model and barotropic tidal currents determined from long-range acoustic transmissions, *Prog. Oceanogr.*, *40*, 337–367.

Egbert, G. D., and S. Y. Erofeeva (2002), Efficient inverse modeling of barotropic ocean tides, *J. Atmos. Oceanic Tech.*, *19*, 183–204.

Han, S.-C., C. Jekeli, and C. K. Shum (2004), Time-variable aliasing effects of ocean tides, atmosphere, and continental water mass on monthly mean GRACE gravity field, *J. Geophys. Res.*, *109*, B04403, doi:10.1029/2003JB002501.

Han, S.-C., C. K. Shum, and K. Matsumoto (2005), GRACE observations of M_2 and S_2 ocean tides underneath the Filchner-Ronne and Larsen ice shelves, Antarctica, *Geophys. Res. Lett.*, *32*, L20311, doi:10.1029/2005GL024296.

Han, S.-C., R. D. Ray, and S. B. Luthcke (2007), Ocean tidal solutions in Antarctica from GRACE inter-satellite tracking data, *Geophys. Res. Lett.*, *34*, L21607, doi:10.1029/2007GL031540.

Hsu, H.-H., and B. J. Hoskins (1989), Tidal fluctuations as seen in ECMWF data, *Q. J. R. Meteorol. Soc.*, *115*, 247–264.

Huthnance, J. M. (1980), On shelf-sea resonance with application to Brazilian M_3 tides, *Deep Sea Res. Part I*, *27*, 347–366.

Klinker, E., F. Rabier, G. Kelly, and J.-F. Mahfouf (2000), The ECMWF operational implementation of four-dimensional variational assimilation. Part III: Experimental results and diagnostics with operational configuration, *Q. J. R. Meteorol. Soc.*, *126*, 1191–1215.

Lambeck, K. (1988), *Geophysical Geodesy*, Clarendon Press, Oxford, U. K.

Llubes, M., and P. Mazzega (1997), Testing recent global ocean tide models with loading gravimetric data, *Prog. Oceanogr.*, *40*, 369–383.

Luthcke, S. B., D. D. Rowlands, F. G. Lemoine, S. M. Klosko, D. Chinn, and J. J. McCarthy (2006), Monthly spherical harmonic gravity field solutions determined from GRACE inter-satellite range-rate data alone, *Geophys. Res. Lett.*, *33*, L02402, doi:10.1029/2005GL024846.

Luthcke, S. B., A. A. Arendt, D. D. Rowlands, J. J. McCarthy, and C. F. Larsen (2008), Recent glacier mass changes in the Gulf of Alaska region from GRACE mascon solutions, *J. Glaciol.*, *54*, 767–777.

Lyard, F., F. Lefèvre, T. Letellier, and O. Francis (2006), Modeling the global ocean tides: Insights from FES2004, *Ocean Dyn.*, *56*, 394–415.

MacArthur, J. L., and A. S. Posner (1985), Satellite-to-satellite range-rate measurement, *IEEE Trans. Geosci. Remote Sens.*, *23*, 517–523.

McCarthy, D. D., and G. Petit (Eds.) (2003), IERS conventions, *IERS Tech. Note 32*, Verl. des Bundesanst. für Kartogr. und Geod., Frankfurt, Germany.

Moore, P., and M. A. King (2008), Antarctic ice mass balance estimates from GRACE: Tidal aliasing effects, *J. Geophys. Res.*, *113*, F02005, doi:10.1029/2007JF000871.

Munk, W. H., and D. E. Cartwright (1966), Tidal spectroscopy and prediction, *Philos. Trans. R. Soc. London Ser. A*, *259*, 533–581.

Padman, L., S. Y. Erofeeva, and H. A. Fricker (2008), Improving Antarctic tide models by assimilation of ICESat laser altimetry over ice shelves, *Geophys. Res. Lett.*, *35*, L22504, doi:10.1029/2008GL035592.

Pedley, M., J. G. Paren, and J. R. Potter (1986), The tidal spectrum underneath Antarctic ice shelves, *J. Geophys. Res.*, *91*, 13,001–13,009.

Peltier, W. R. (2004), Global glacial isostatic adjustment and the surface of the ice-age Earth: The ICE-5G model and GRACE, *Annu. Rev. Earth Planet. Sci.*, *32*, 111–149.

Ray, R. D. (1999), A global ocean tide model from TOPEX/POSEIDON altimetry: GOT99.2, *Rep. NASA/TM-1999-209478*, 58 pp., Goddard Space Flight Cent., Greenbelt, Md.

Ray, R. D. (2001), Comparisons of global analyses and station observations of the S_2 barometric tide, *J. Atmos. Solar Terr. Phys.*, *63*, 1085–1097.

Ray, R. D., and G. D. Egbert (2004), The global S_1 tide, *J. Phys. Oceanogr.*, *34*, 1922–1935.

Ray, R. D., and S. B. Luthcke (2006), Tide model errors and GRACE gravimetry: Towards a more realistic assessment, *Geophys. J. Int.*, *167*, 1055–1059.

Ray, R. D., and R. M. Ponte (2003), Barometric tides from ECMWF operational analyses, *Ann. Geophys.*, *21*, 1897–1910.

Ray, R. D., R. J. Eanes, and F. G. Lemoine (2001), Constraints on energy dissipation in the Earth's body tide from satellite tracking and altimetry, *Geophys. J. Int.*, *144*, 471–480.

Ray, R. D., D. D. Rowlands, and G. D. Egbert (2003), Tidal models in a new era of satellite gravimetry, *Space Sci. Rev.*, *108*, 271–282.
Rodell, M., et al. (2004), The global land data assimilation system, *Bull. Am. Meteorol. Soc.*, *85*, 381–394.
Rowlands, D. D., R. D. Ray, D. S. Chinn, and F. G. Lemoine (2002), Short-arc analysis of intersatellite tracking data in a gravity mapping mission, *J. Geod.*, *76*, 307–316.
Savcenko, R., and W. Bosch (2008), EOT08a—Empirical ocean tide model from multi-mission satellite altimetry, *Rep. 81*, 37 pp., Dtsch. Geod. Forschungsinst, Munich.
Schrama, E. J. O., B. Wouters, and D. A. Lavallée (2007), Signal and noise in Gravity Recovery and Climate Experiment (GRACE) observed surface mass variations, *J. Geophys. Res.*, *112*, B08407, doi:10.1029/2006JB004882.
Tapley, B. D., S. Bettadpur, J. Ries, P. Thompson, and M. Watkins (2004), GRACE measurements of mass variability in the Earth system, *Science*, *305*, 503–505.
Tapley, B. D., et al. (2005), GGM02—An improved Earth gravity field model from GRACE, *J. Geod.*, *79*, 467–478.
Van den Dool, H., S. Saha, J. Schemm, and J. Huang (1997), A temporal interpolation method to obtain hourly atmospheric surface presure tides in Reanalysis 1979–1995, *J. Geophys. Res.*, *102*, 22,013–22,024.
Wolff, M. (1969), Direct measurements of the Earth's gravitational potential using a satellite pair, *J. Geophys. Res.*, *74*, 5295–5300.

J.-P. Boy, S. B. Luthcke, and R. D. Ray, NASA Goddard Space Flight Center, Mail Code 698, Greenbelt, MD 20771, USA. (richard.ray@nasa.gov)